Heat Transfer Characteristics of an Inclined Impinging Jet on a Curved Surface in Crossflow

Article *in* Journal of Heat Transfer · April 2014

DOI: 10.1115/1.4027389

CITATIONS
3

READS
43

5 authors, including:

X.L. Wang
Nanjing JiuDing Refrigeration & Air-condition…
4 PUBLICATIONS **16** CITATIONS
SEE PROFILE

Hongbin Yan
Northwestern Polytechnical University
10 PUBLICATIONS **31** CITATIONS
SEE PROFILE

Tian Jian Lu
Xi'an Jiaotong University
551 PUBLICATIONS **8,635** CITATIONS
SEE PROFILE

X. L. Wang
State Key Laboratory for Mechanical Structure Strength and Vibration,
Xi'an Jiaotong University,
Xi'an 710049, China
e-mail: wanglong12346@163.com

H. B. Yan
School of Energy and Power Engineering,
Xi'an Jiaotong University,
Xi'an 710049, China
e-mail: hongbin.1988@stu.xjtu.edu.cn

T. J. Lu
State Key Laboratory for Mechanical Structure Strength and Vibration,
Xi'an Jiaotong University,
Xi'an 710049, China
e-mail: tjlu@mail.xjtu.edu.cn

S. J. Song[1]
School of Mechanical and Aerospace Engineering,
Seoul National University,
Seoul 151-742, South Korea
e-mail: sjsong@snu.ac.kr

T. Kim[1]
School of Mechanical Engineering,
University of the Witwatersrand,
Johannesburg 2050, South Africa
e-mail: tong.kim@wits.ac.za

Heat Transfer Characteristics of an Inclined Impinging Jet on a Curved Surface in Crossflow

This study reports on heat transfer characteristics on a curved surface subject to an inclined circular impinging jet whose impinging angle varies from a normal position $\theta = 0$ deg to $\theta = 45$ deg at a fixed jet Reynolds number of $Re_j = 20{,}000$. Three curved surfaces having a diameter ratio (D/D_j) of 5.0, 10.0, and infinity (i.e., a flat plate) were selected, each positioned systematically inside and outside the potential core of jet flow where D_j is the circular jet diameter. Present results clarify similar and dissimilar local heat transfer characteristics on a target surface due to the convexity. The role of the potential core is identified to cause the transitional response of the stagnation heat transfer to the inclination of the circular jet. The inclination and convexity are demonstrated to thicken the boundary layer, reducing the local heat transfer (second peaks) as opposed to the enhanced local heat transfer on a flat plate resulting from the increased local Reynolds number. [DOI: 10.1115/1.4027389]

Keywords: circumferential heat transfer, convexity, inclined jet, potential core, transition

1 Introduction

The superior heat transfer performance of impinging jets for cooling or heating compared to other convective heat transfer schemes has led to a variety of practical applications. Therefore, a multitude of studies on momentum, heat, and mass transfer by impinging jet flows have been reported, considering hydrodynamic [1–3], thermal [4,5] or geometric aspects [6–8]. It has been shown that overall and local heat transfer characteristics on a flat plate depend strongly on a stream-wise distance from a jet exit—an impinging distance, among other parameters [1,9–12]. The highest heat transfer typically occurs at a stagnation point on a flat plate coinciding with the jet axis—a primary peak, at low turbulence levels and low Reynolds number ranges [13,14]. Depending on the impinging distance relative to the potential core of jet flow, either two peaks of local heat transfer (a primary peak at the stagnation point and a second peak off from the stagnation point) or a single peak (only a primary peak at the stagnation point) exist. Locally, the appearance and disappearance of the second peak are associated with the presence of the laminar to turbulent transition of jet flow.

In some applications, jet impingement is oblique rather than normal to a target surface due to the shape of target surfaces or to constraints on the positioning of the jet. As the jet axis is inclined from its normal position, there is a lateral shift of the primary peak which initially coincides with a geometric stagnation point (defined as the intersection of the jet axis and the target surface) toward the so-called "uphill side" [15–21] as illustrated in Fig. 1. With inclination, two conflicting observations have been made: the increased primary peak (Fig. 1(*a*)) and the decreased primary peak (Fig. 1(*b*)) while both are laterally shifted toward the uphill side.

Akansu et al. [15] experimentally observed a monotonic increase in the stagnation heat transfer on a flat plate with increasing an oblique angle while its lateral shift toward the uphill side was accompanied, at a small impinging distance ($z/(2b) = 2.0$), where z is the jet axis and b is the slot width. Tong [19] performed a numerical study on an oblique slot liquid jet heat transfer on a flat plate at the impinging distance of 3 slot width. The results show that with a uniform jet flow profile, the peak Nusselt number increases as the jet is inclined from a normal position, whereas the peak Nusselt number initially declines and eventually rises with a parabolic jet flow profile.

An opposite response of the primary peak's magnitude to inclination has also been observed as illustrated in Fig. 1(*b*). Goldstein and Franchett [16] conducted experiments to determine heat transfer by a circular impinging jet at different inclination angles on a flat plate. For the impinging distance (z) of 4–10D_j, a decrease in the primary peak with larger inclination angles was found, where D_j is the jet diameter. Similar observation was reported by Beitelmal et al. [17] who experimentally investigated an inclined impinging slot jet removing heat from a uniformly heated flat plate for the impinging distance ranging from 4 to 12 times of the hydraulic diameter of the slot.

It seems that the inclination of both slot and circular jets from their normal position causes either the increased peak heat transfer or the decreased peak heat transfer while its lateral shift toward the uphill side is in common. However, there is a hint that the impinging distance, z/D_j especially its relative location to the

[1]Corresponding authors.

Contributed by the Heat Transfer Division of ASME for publication in the Journal of Heat Transfer. Manuscript received October 3, 2013; final manuscript received April 2, 2014; published online April 23, 2014. Assoc. Editor: Giulio Lorenzini.

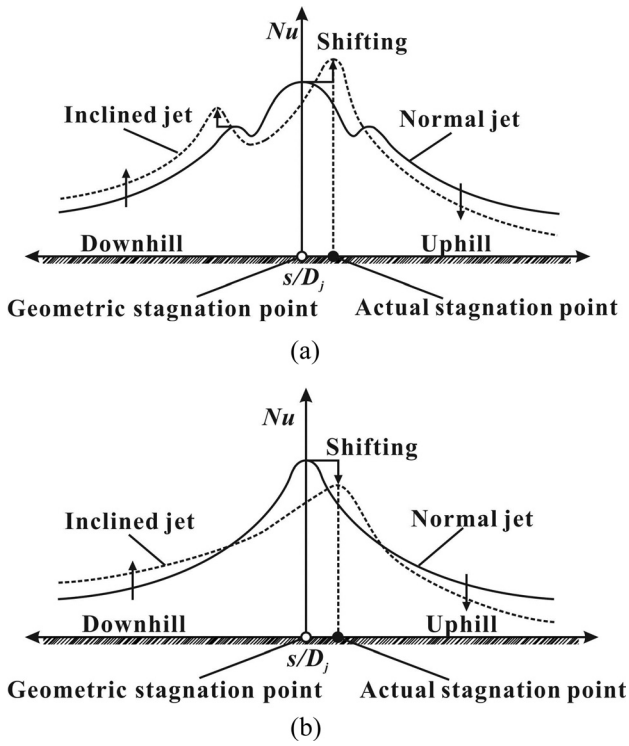

Fig. 1 Schematic summary illustrating how the inclination of a single jet affects lateral heat transfer distribution on a flat plate [6–11]; (*a*) for a "small" impinging distance; (*b*) for a "large" impinging distance

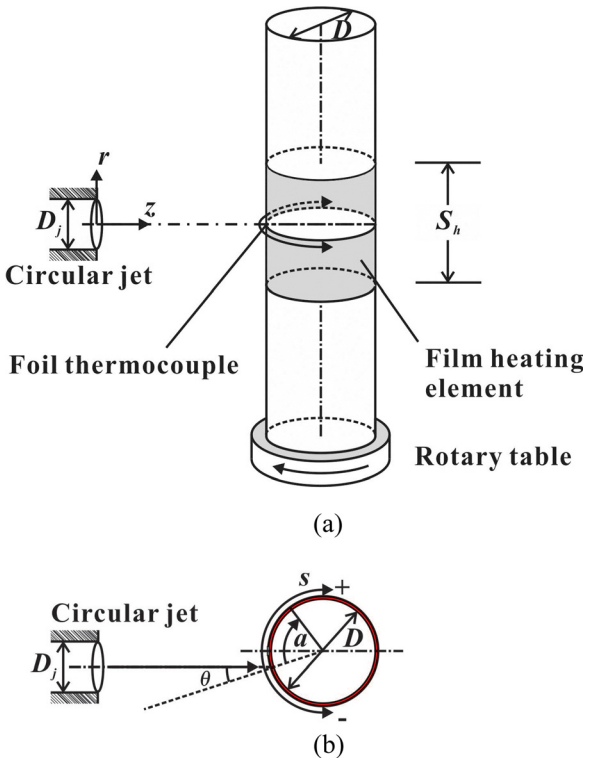

Fig. 3 Schematics of (*a*) test setup for measuring heat transfer distribution along the circumference of a heated circular cylinder cooled by an inclined jet; (*b*) a crossflow plane

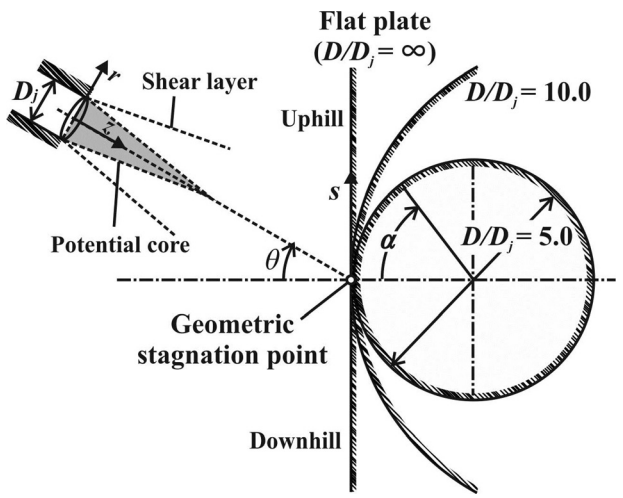

Fig. 2 Schematic of an inclined circular jet impinging on curved surfaces e.g., circular cylinders where a flat plate has an infinite radius

potential core length of a given jet is a key parameter that determines the observed two distinctive responses, which needs to be clarified.

Unlike the impinging jet on a flat plate, relatively few studies have been concerned with an inclined impinging jet on a curved surface (e.g., a circular cylinder) despite its engineering importance. Thus far, observations made on circumferential heat transfer characteristics on a circular cylinder (or a convex surface) impinged by a normal jet [22–28] are: (a) when positioned close to the jet exit, a second peak, in addition to a primary peak at the stagnation point, forms; (b) a second peak disappears when positioned relatively far away from the jet exit along the jet axis and (c) flow separation causes a local heat transfer minimum on small target cylinders while transition from laminar to turbulent flow causes a second peak on large target cylinders. Among these few studies on the inclined jet, Lim et al. [29] measured local heat transfer coefficients on a hemispherical convex surface with a round oblique impinging jet for $2.0 \le z/D_j \le 10.0$ and $0\,\text{deg} \le \theta \le 40\,\text{deg}$ at a fixed jet Reynolds number of 23,000. Here, θ denotes the angle that is inclined from the axis normal to the tangent of the curved surface at its geometric stagnation point. The results show that the azimuthal shift of the primary peak that initially coincides with the geometric stagnation point is more pronounced with a larger inclination angle and a shorter impinging distance. Tawfek [30] who experimentally investigated an obliquely impinging round jet on a circular cylinder observed that the azimuthal location of the primary peak is shifted toward the uphill side, which is consistent with that observable on a flat plate.

Thus far, some local heat transfer characteristics on a flat plate and their similar and dissimilar characteristics on curved surfaces, both subject to a single circular impinging jet have not yet been fully understood. This study, therefore, aims to squarely address the following specific issues:

(a) How does the inclination affect local heat transfer characteristics on curved surfaces (i.e., cylinders) compared to those on a flat plate, which could be considered as a cylinder with an infinite radius?
(b) How and why does the convexity of target surfaces alter local heat transfer characteristics?
(c) What does a short or long impinging distance specifically refer to in both a flat plate and curved surfaces?

To address these specific issues, a series of experiments on a circular cylinder positioned at selected downstream positions for a fixed jet Reynolds number of $\text{Re}_j = 20{,}000$ have been conducted. Two selected cylinders with $D/D_j = 5.0$ and 10.0 are tested for a fixed D_j (Fig. 2). As reference, a circular impinging jet on a uniformly heated flat plate (i.e., $D/D_j = \infty$) is also considered. Heat

Table 1 Parameters of test setup and conditions

Test parameter	Value
Circular jet diameter, D_j	0.026 m
Circular cylinder diameter, D	0.13 m, 0.26 m, infinity (a flat plate)
Relative radius ratio, D/D_j	5.0, 10.0, Infinity (a flat plate)
Mass flow rate, $\dot{m}$	0.0065 kg/s
Reynolds number, Re_j	20,000
Width of heating element, S_h	0.20 m
Constant heat flux, q	1428 W/m^2

transfer and pressure coefficients along the circumference of each cylinder and on a flat plate are measured. Prior to measurements, the jet flow characteristics such as the potential core length were measured for the present circular jet.

2 Experimental Details

2.1 Test Rig and Instrumentation. Figure 3 shows a schematic of the present test rig consisting of a circular jet nozzle, an air supply system, and a target curved surface (a cylinder/a flat plate). Air at ambient conditions drawn by a centrifugal fan was discharged from the circular jet with a fixed diameter of $D_j = 26$ mm. The mass flow rate through the jet nozzle was calculated based on the measured velocity profile at the circular jet exit. The jet Reynolds number Re_j (based on the jet diameter D_j and mean jet velocity) was fixed at 20,000. The circular jet was mounted on a linear traverse system so that the impinging distance z/D_j could be varied systematically.

The centerline velocity of the jet flow along the jet axis (the z-axis) in a free exit was measured to quantify the potential core length, using a pitot tube mounted on an automated linear traverse system. Pressure readings from the stagnation and static tappings were recorded by a differential pressure transducer. In addition, the radial profile of the axial velocity component of the jet flow was traversed at selected downstream planes.

Boundary layer thickness (δ) was measured normal to a target surface at selected lateral (azimuthal) locations by traversing a boundary layer probe with a tip thickness of 0.5 mm in conjunction with a static pressure probe. The both probes were traversed separately with an increment of 0.2 mm to resolve thin boundary layer.

For heat transfer measurement, a film-type heating element with a thickness of 0.32 mm that simulates constant heat flux was attached to the outer surface of a target cylindrical perspex tube having its outer diameter of D (listed in Table 1). The thickness of the tube was 5.0 mm and the target cylinder was filled with a low thermally conducting foam as a thermal insulation to minimize heat loss. The net heat flux, q'' was estimated as

$$q'' = q''_{\mathrm{input}} - q''_{\mathrm{cond}} - q''_{\mathrm{rad}} \tag{1}$$

where q''_{input} is the input heat flux from the film-type heater calculated based on the input current (I) and voltage (V) from a DC power supply to the heater ($q''_{\mathrm{input}} = \mathrm{IV}$), and q''_{cond} and q''_{rad} are respectively the heat losses via conduction and radiation. The conductive heat loss occurring through the target cylinder's thickness was estimated using Fourier's law. The radiative heat loss was calculated by Stefan–Boltzmann's law as

$$q''_{\mathrm{rad}} = \varepsilon\sigma(T_s^4 - T_a^4) \tag{2}$$

where ε is the emissivity, σ is the Stefan–Boltzmann constant, T_s is the cylinder surface temperature, and T_a is the ambient temperature. The surface of the target cylinder was painted in black and the emissivity was obtained during the in-situ calibration of an infrared (IR) camera and estimated to be $\varepsilon = 0.98$ by adjusting the emissivity setup to match the cylinder temperature readings from flush mounted film-type thermocouples.

During the experiment on a cylinder, the target cylinder was rotated with a 10 deg increment to cover the cylinder circumference from $\alpha = 0$ deg (the geometric stagnation point) to $\alpha = 350$ deg. Note that no flow disturbance or change by the surface mounted film thermocouples was assumed due to their thinness. A bead T-type thermocouple was also used to monitor the jet exit temperature (T_j). Prior to the measurements, each thermocouple was calibrated in a container filled with an ice-water mixture.

As reference, the distribution of surface temperatures on the flat plate was measured using a pre-calibrated IR camera. Thermal images were further corrected for a non-perpendicular viewing angle during the post-image process. The flat plate was painted in black to reduce the reflectivity. The backside of the flat plate was insulated thermally to minimize heat loss.

2.2 Data Reduction Parameters and Measurement Uncertainties. The jet Reynolds number based on the jet diameter D_j and mean jet velocity w_m measured at the jet exit, is defined as

$$\mathrm{Re}_j = \frac{\rho w_m D_j}{\mu} \tag{3}$$

During the entire experiment, the jet Reynolds number was fixed at 20,000.

The local static pressure distribution was evaluated using the dimensionless pressure coefficient defined as

$$C_p(\alpha) = \frac{p(\alpha) - p_e}{\rho w_e^2/2} \tag{4}$$

where $p(\alpha)$ and p_e are the static pressures measured on the target surface at an arbitrary lateral (azimuthal) location and at the jet exit, respectively.

The heat transfer characteristics were evaluated using the Nusselt number defined based on the jet diameter D_j as

$$Nu(\alpha) = \frac{h(\alpha)}{k_f/D_j} \tag{5}$$

where

$$h(\alpha) = \frac{q''}{T_s(\alpha) - T_j} \tag{6}$$

Here, q'' is the estimated net heat flux (Eq. (1)), k_f is the thermal conductivity of air while T_s and T_j are the local surface temperature and jet flow temperature at the jet exit $z = 0$, respectively. The origin of the azimuth angle α coincided with the geometric stagnation point.

The uncertainty associated with the azimuth angle was found to be within $\pm$ 0.2 deg. The measurement uncertainties of the Reynolds number and the static pressure coefficient were estimated using a method reported in Ref. [31] (based on 20:1 odds) and found to be within 1.3% and 2.8%, respectively. The uncertainty of the velocity measurement inside the boundary layer was estimated to be within 5.0%. The resolution of the temperature readings from the temperature scanner was found to be $\pm$0.1 K for each thermocouple.

The estimation of the heat loss via conduction and radiation showed that approximately 1% (conduction) and 12% (radiation) of the input heat was lost. The uncertainty of the Nusselt number was then calculated to be within 5.1%. In the present temperature range, the deviation of the IR camera measured temperature from that measured by the thermocouple was calculated to be $\pm$0.2 K. Hence, the temperature uncertainty was estimated to be within $\pm$0.3 K. Consequently, the uncertainty of the Nusselt number on

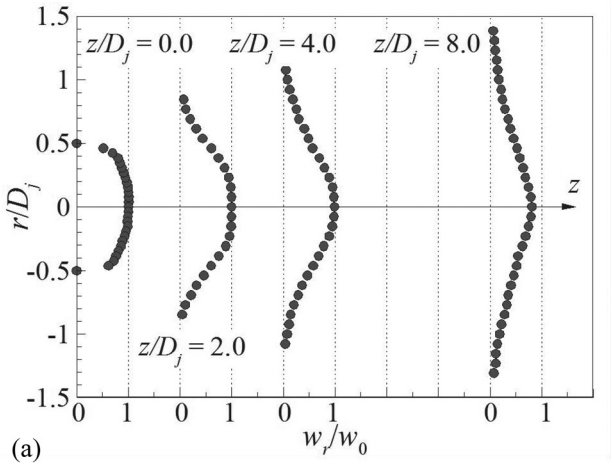

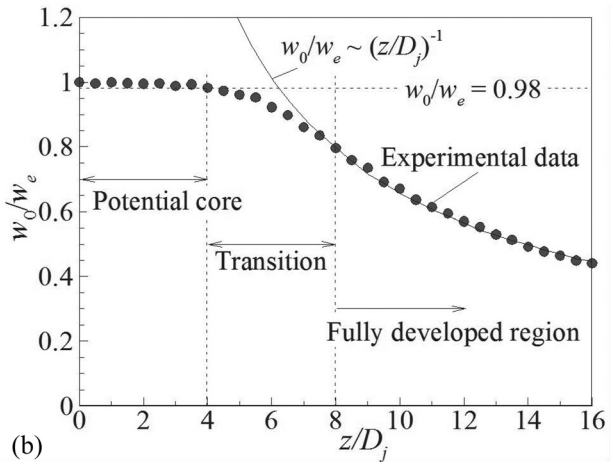

Fig. 4 Free jet characteristics of a circular jet at $Re_j = 20{,}000$; (*a*) radial profiles of axial velocity at selected downstream transverse planes; (*b*) variation of normalized centerline velocity along the jet axis (i.e., the *z*-axis), indicating a potential core persisting up to $z/D_j = 4.0$

the flat plate mapped by the IR camera was calculated to be within 5.8%.

3 Discussion of Results

3.1 Circular Jet Characteristics in Free Exit. The potential core length and velocity profile indicates the jet flow characteristics that subsequently influence local and overall heat transfer on a target surface downstream. Figure 4(*a*) exhibits the radial profiles of the axial velocity component at selected traverse planes and indicates a symmetric flow field with respect to the jet axis. According to the classical description of free jet flow structures [32], there exist three distinctive flow regions: (a) the initial region, (b) the transitional region, and (c) the fully developed region. In the initial region, the jet velocity along the jet axis maintains its magnitude as high as that at the jet exit. Furthermore, a region where the jet flow is undisturbed by the flow interaction with the surrounding fluid at rest (submerged jet) is present, the so-called "potential core." For circular jets, Martin [9] suggested that the core length persists up to $4D_j$, while Gautner et al. [1] reported that it typically ranges from $4.7D_j$–$7.7D_j$. After the jet flow is fully developed via transition, the axial velocity profiles become self-similar, collapsing onto a single curve that could be fitted using Gaussian distribution [33].

The potential core length of the present circular jet in the free exit was quantified by traversing the centerline jet velocity w_0 at

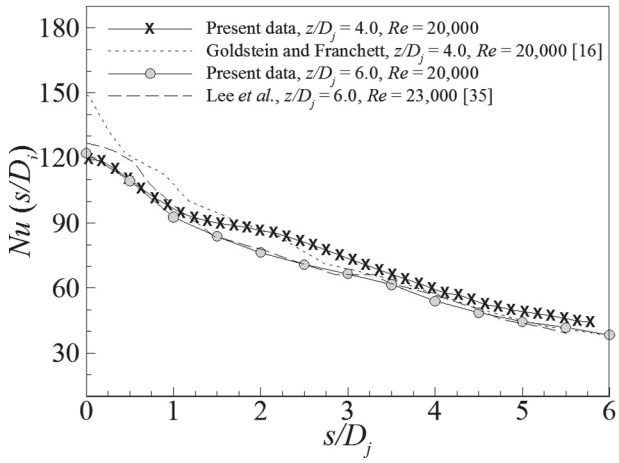

Fig. 5 Comparison of lateral heat transfer distributions on a flat plate subject to a normal impinging jet to the data reported by Goldstein and Franchett [16] and Lee et al. [35]

$r = 0$. Figure 4(*b*) shows the centerline velocity normalized by that measured at the jet exit, w_e. Following the definition of Giralt et al. [34] that the potential core length is the distance from a nozzle exit to a downstream location where the centerline velocity w_0 reaches 98% of the jet exit velocity w_e, it is derived from Fig. 4 that the present free jet has the potential core length $z/D_j = 4.0$. Inside the potential core ($z/D_j \leq 4.0$), the centerline velocity has the same magnitude as w_e. Outside the potential core (i.e., $z/D_j > 4.0$), the axial centerline velocity w_0 decays inversely proportional to the axial distance [32], as

$$\frac{w_0}{w_e} \sim \left(\frac{z}{D_j}\right)^{-1} \tag{7}$$

The measured centerline velocity data followed the trend expressed by Eq. (7) after $z/D_j = 8.0$. According to Abramovich and Schindel [32], the onset of the fully developed region (or self-similar region) occurs approximately at $z/D_j = 8.0$.

It should be noted that the flow characteristics of the present jet in the free exit (Fig. 4) are expected to vary due to the presence of a target cylinder downstream, but assumed to be consistent among the considered cases. It has been argued [13,14] that the jet flow structure affected by the presence of a target surface is limited within approximately $1.0D_j$ upstream and other flow regions remain unaffected, which may hold for the present configuration.

3.2 Heat Transfer Characteristics on a Reference Flat Plate ($D/D_j = \infty$). Heat removal from a flat plate by an inclined circular jet or a slot jet has long been studied [15–20]. Some conclusions made on local heat transfer characteristics are summarized as follows. When the jet is inclined from its normal impinging position, there is either an increase or a decrease in the primary peak (i.e., its magnitude): the increased peak heat transfer is observable when the flat plate is positioned "close" to the jet exit [15,19] while the opposite is achievable when positioned relatively "far away" from the jet exit [16,17]. In both cases, the lateral shift of the primary peak toward the uphill side is in common. Furthermore, the second peak in addition to the primary peak is formed only if the flat plate is close to the jet exit, which is associated with the presence of laminar to turbulent transition on the flat plate.

This section serves firstly to confirm these previous observations as reference, second to clarify a key parameter that causes the observed opposite (or transitional) response of the primary peak (i.e., its magnitude) to the inclination, and lastly to provide

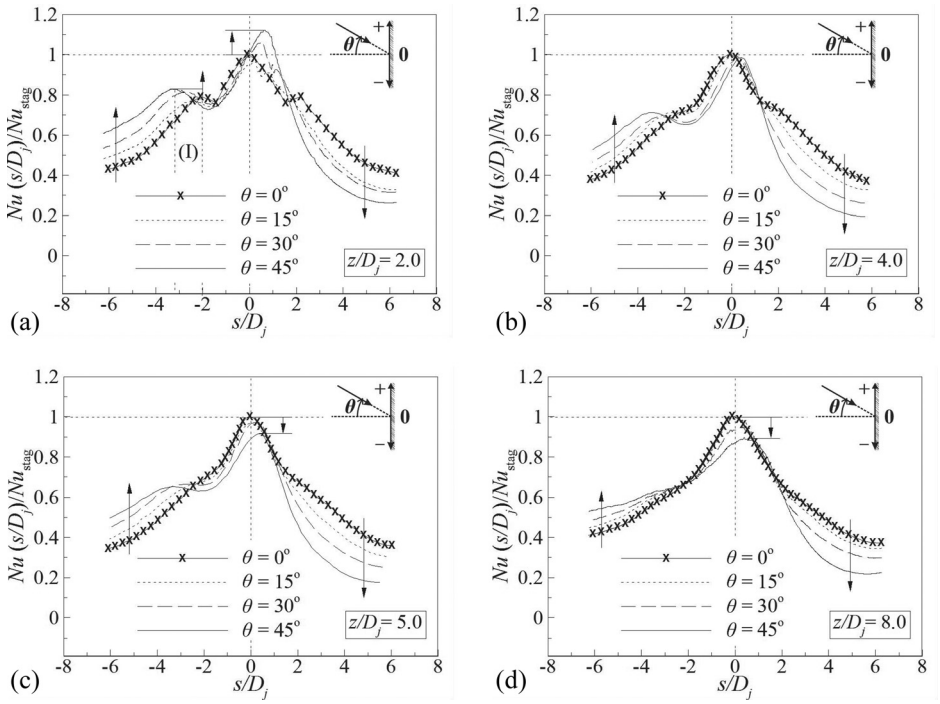

Fig. 6 Lateral heat transfer distribution on a flat plate subject to an inclined jet at $Re_j = 20{,}000$ with four selected inclination angles with the potential core persisting up to $z/D_j = 4.0$; (*a*) $z/D_j = 2.0$ (inside potential core); (*b*) $z/D_j = 4.0$ (at potential core tip); (*c*) $z/D_j = 5.0$ (slightly outside potential core; (*d*) $z/D_j = 8.0$ (outside potential core)

the mechanisms of newly found local heat transfer characteristics in the present study.

3.2.1 Shifting of the Primary Peak. Before proceeding further, it is instructive to provide the credibility of the present experimental setup. To this end, lateral heat transfer distributions on a flat plate positioned at $z/D_j = 4.0$ and 6.0 are compared to the data reported in Refs. [16,35] for the normal impinging jet position ($\theta = 0$ deg). Good agreement is obtained in Fig. 5 except a slight deviation in the stagnation region, which may be caused by different turbulence levels at the jet exit (Gardon and Akfirat [13]).

Figure 6(*a*) plots the lateral heat transfer distribution on Figure 6(*a*) plots the lateral heat transfer distribution on the flat plate which is at $z/D_j = 2.0$ (inside the potential core), for four selected inclination angles ($\theta = 0$ deg, 15 deg, 30 deg, and 45 deg). To facilitate the comparison, the local Nusselt number was normalized by that measured at the stagnation point for $\theta = 0$ deg, denoted as Nu_{stag}. At $\theta = 0$ deg, the local heat transfer peaks at the stagnation point i.e., $\alpha = 0$ deg, forming the primary peak. As the inclination angle increases up to $\theta = 45$ deg, the primary peak moves toward the uphill side and its magnitude is increased.

With the flat plate near the tip of the potential core ($z/D_j = 4.0$), the inclination only causes the lateral shift of the primary peak toward the uphill side, Fig. 6(*b*): the magnitude of the primary peak remains unchanged. For the flat plate slightly downstream of the potential core ($z/D_j = 5.0$), the magnitude of the primary peak is decreased, while its consistent lateral shift toward the uphill side is evident in Fig. 6(*c*). Positioning the flat plate farther downstream e.g., $z/D_j = 8.0$ does not cause any further changes (Fig. 6(*d*)).

In previous studies, the lateral shift of the primary peak toward the uphill side has been univocal [15–20]. However, on the effects of the inclination on the magnitude of the primary peak, two conflicting observations have been reported: the increased inclination angle from the normal position leads to its increase [15,19] or its decrease [16,17]. Based on the present systematic study, it can be clarified that if the flat plate is positioned inside the potential core of the jet flow, the primary peak is increased with the inclination

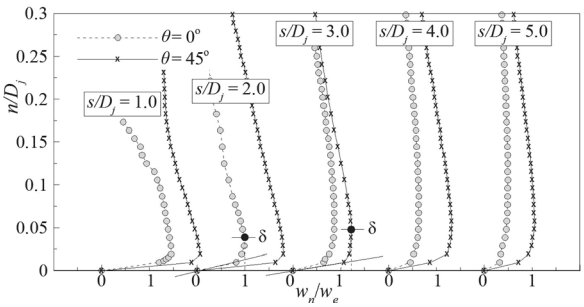

Fig. 7 Velocity profiles measured at selected lateral locations on the downhill side positioned at $z/D_j = 2.0$

whereas outside the potential core, the primary peak is decreased. There is a transition near the tip of the potential core in which no change of the primary peak in magnitude is taken place while its shift toward the uphill side is consistent.

3.2.2 Formation of the Second Peak. A second peak of local heat transfer on the flat plate is formed at $s/D_j = 2.0$. Its formation is known to be associated with the occurrence of laminar to turbulent transition [13]. The present results in Fig. 6 indicate that both the impinging distance (z/D_j) and the inclination angle (θ) are influential.

At $z/D_j = 2.0$ (inside the potential core) and $\theta = 0$ deg (no inclination), the second peak is formed in both the uphill and downhill sides. As the jet is inclined, the second peak on the uphill side disappears whereas that on the downhill side remains. The magnitude of the second peak is increased as well. The laminar to turbulent transition appears to be delayed: an elongated distance from the actual stagnation point (i.e., the primary peak) to the local heat transfer minimum on the downhill side.

Near the tip of the potential core (i.e., $z/D_j = 4.0$), there is no obvious second peak with no inclination (at $\theta = 0$ deg) as depicted in Fig. 6(*b*). However, as the jet is inclined, the second peak

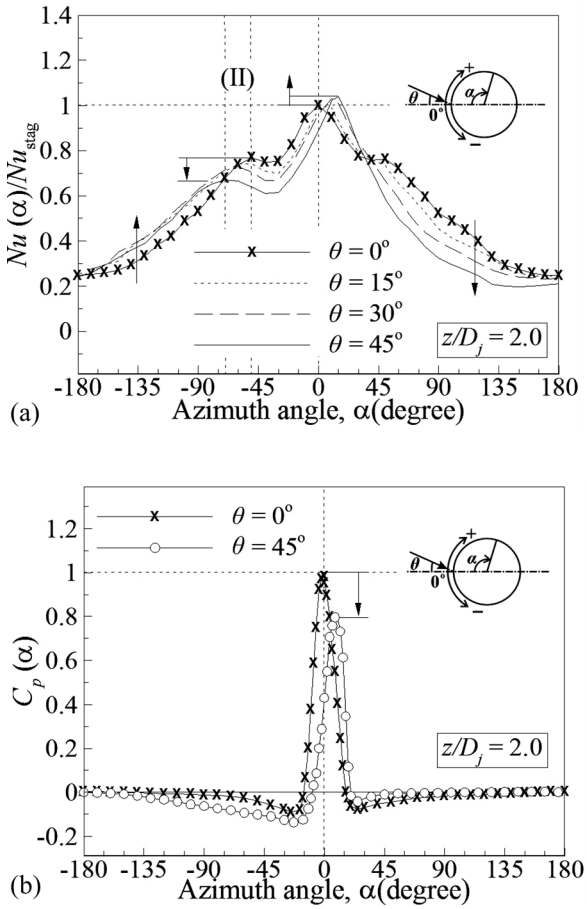

Fig. 8 Circumferential distribution of (*a*) heat transfer and (*b*) static pressure on a target cylinder ($D/D_j = 5.0$) positioned inside the potential core at $Re_j = 20{,}000$

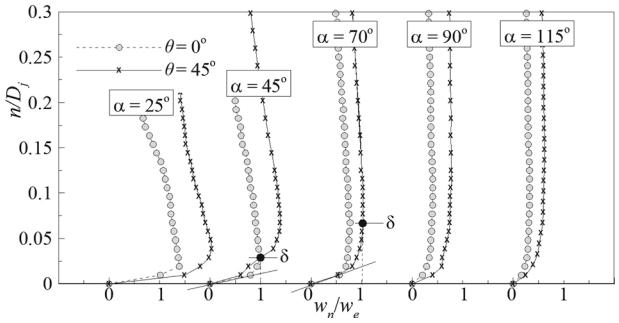

Fig. 9 Velocity profiles measured at selected azimuth angles in the downhill side at $z/D_j = 2.0$

begins to develop only on the downhill side. Especially at $\theta = 45$ deg, the second peak becomes obvious. However, outside the potential core (Figs. 6(*c*) and 6(*d*)), the second peak disappears on both sides regardless of the inclination angle.

The cause of the increased heat transfer at the second peak as a result of the jet's inclination has not yet been fully understood. Momentum boundary layer measurement conducted by Vipat et al. [6] shows that the inclination causes the uneven flow distribution on the uphill and downhill sides on a flat plate subject to the slot jet impingement: a higher momentum on the downhill side than on the uphill side exists. The present boundary layer data measured at the selected lateral locations on a flat plate where the second peak is formed i.e., $s/D_j = 2.0$ for $\theta = 0$ deg and $s/D_j = 3.0$ for $\theta = 45$ deg (Fig. 7) reveals that the momentum on the downhill side is increased but the thickness of boundary layer (δ) remains almost unchanged e.g., $n/D_j \sim 0.05$ when the jet is inclined (Fig. 7). Here, the boundary layer thickness δ is typically defined as the distance between the surface and the velocity maximum [36]. The increased momentum leads to an increase in the local Reynolds number, resulting in a larger velocity gradient on the flat plate. This implies the increased wall shear stress as indicated in Fig. 7. Consequently, the local heat transfer at the second peak is enhanced as the jet is inclined (or as the inclination angle is increased).

3.3 Heat Transfer Characteristics on a Curved Surface ($D/D_j = 5.0$). Heat transfer characteristics on a cylinder with a finite diameter ratio e.g., $D/D_j = 5.0$ subject to the same circular jet in crossflow are considered. Due to the radius of the cylinder which changes a viewing angle to the fixed IR camera's position dramatically, exhaustive corrections to compensate the curvature are required. Therefore, a film-type thermocouple flush mounted on the cylinder surface was used instead. An automated rotation of the cylinder allows a full azimuthal coverage of the local heat transfer data. The jet Reynolds number was set to be $Re_j = 20{,}000$.

3.3.1 Inside the Potential Core. With the target cylinder inside the potential core of the jet flow ($z/D_j = 2.0$) at the normal impinging position ($\theta = 0$ deg), a symmetric local heat transfer distribution in the crossflow plane is seen in Fig. 8(*a*). The highest heat transfer coincides with the geometric stagnation point ($\alpha = 0$ deg). The local heat transfer is decreased until $\alpha = 30$ deg having a local minimum, followed by a slight increase up to $\alpha = 50$ deg where a second peak is formed. After which, the local heat transfer is monotonically decreased. This overall distribution is qualitatively consistent with that observed on the flat plate.

As the circular jet is inclined from the normal position, the changes in the local heat transfer distribution are similar to those observed on the flat plate such as (a) the azimuthal shift of the primary peak toward the uphill side, (b) the increase in its magnitude, (c) the disappearance of the second peak on the uphill side, (d) the decreased local heat transfer on the uphill side while the increased local heat transfer on the downhill side, and (e) the delayed laminar to turbulent transition from the actual stagnation point on the downhill side. However, there also exist differences in the local heat transfer characteristics such as (a) the uphill side heat transfer distribution is more sensitive to the inclination than the downhill side as opposed to the equal sensitivity on the flat plate and (b) on the rear cylinder surface the local heat transfer values become similar regardless of the inclination angles.

A more distinct difference is the magnitude of the second peak on the downhill side that is decreased in contrast to the observed increase on the flat plate (Fig. 6(*a*)). Since the target surface is convexed, the flow on the cylinder surface turns, inducing an additional force i.e., the centrifugal force. The static pressure distributed along the circumference of the cylinder (Fig. 8(*b*)) indicates that the flow on the cylinder surface is attached since flow separation does not occur.

Figure 9 shows the velocity profiles measured at selected azimuthal locations including those coinciding with the second peak at $\alpha = 45$ deg for $\theta = 0$ deg and $\alpha = 45$ deg for $\theta = 45$ deg (denoted as (II) in Fig. 8(*a*)). A change in the maximum velocity at the two azimuthal locations is negligible although the jet is inclined. However, the thickness of boundary layer is almost doubled. The thickened boundary layer then causes the decrease in the local heat transfer at the second peak as observed in Fig. 9. It should be noted that on the flat plate the boundary layer thickness remains the same while the maximum velocity is increased as a result of the inclination, resulting in the enhanced local heat transfer.

In summary, the inclination of a circular jet impinging on a curved surface (cylinder) causes the thickening of the boundary layer. As a result, the local heat transfer at the second peak is decreased.

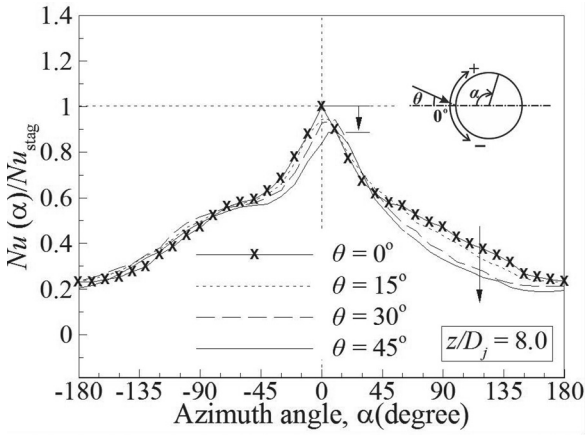

Fig. 10 Circumferential distribution of heat transfer on a target cylinder ($D/D_j = 5.0$) positioned outside the potential core at $Re_j = 20{,}000$

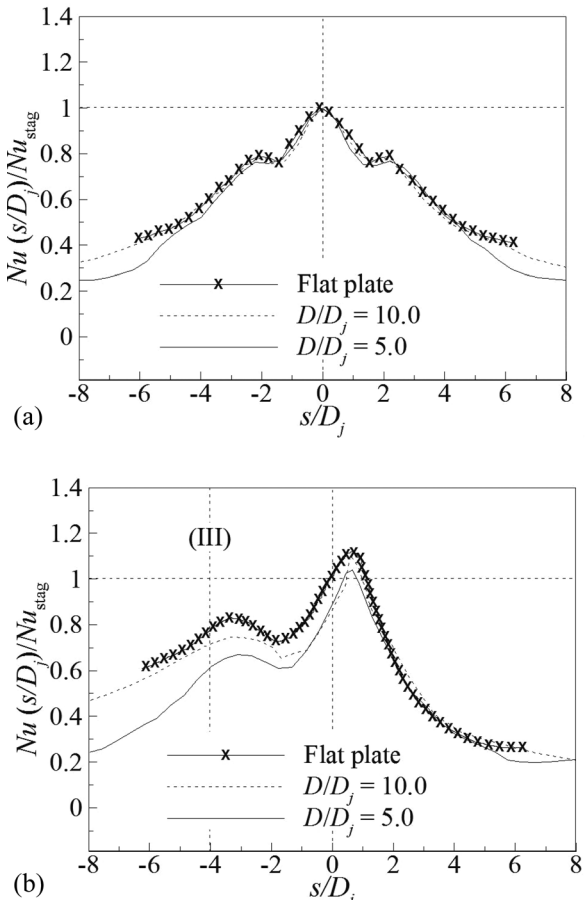

Fig. 11 Lateral heat transfer distribution on curved surfaces subject to an inclined impinging jet at $z/D_j = 2.0$ and $Re_j = 20{,}000$: (*a*) $\theta = 0$ deg and (*b*) $\theta = 45$ deg

3.3.2 Outside the Potential Core. The results in Fig. 10 exhibit local heat transfer distribution on the cylinder positioned outside the potential core ($z/D_j = 8.0$) showing the disappearance of the second peak. The decrease in the primary peak and its azimuthal shift toward the uphill side are also consistent with those observed on the flat plate. One noticeable feature is almost invariant local heat transfer on the downhill side while a decrease of the local heat transfer on the uphill side is evident as the inclination angle is increased.

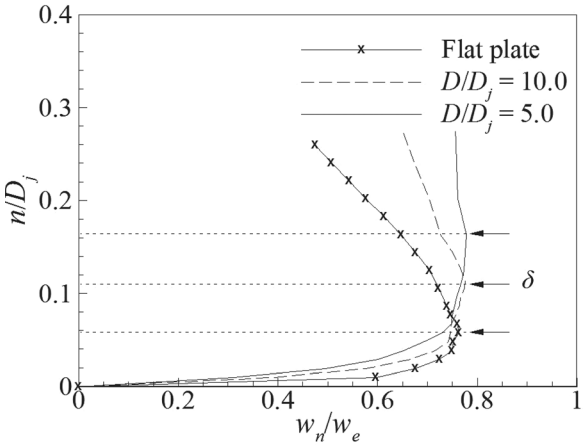

Fig. 12 Velocity profiles measured at $s/D_j = 4.0$ (denoted as (III) in Fig. 10(*b*)) on two cylinders and a flat plate positioned at $z/D_j = 2.0$ (denoted as (III) in Fig. 10(*b*))

The disappearance of the second peak on the flat plate that is positioned outside the potential core has been argued by Jambunathan et al. [10] as follows. A series of toroidal vortices that form in the shear region around the circumference of the jet are convected downstream. Subsequently, these vortices merge into large vortices and brake down into small-scale random turbulence that penetrates into the jet axis. This penetration causes the radial (or lateral) oscillation of flow on the flat plate, resulting in the breakdown of any distinct flow features including flow transition from laminar to turbulent flow. This argument seems to hold for the impinging jet on to the circular cylinder.

3.4 Effects of the Convexity. The alteration of local heat transfer characteristics due to the convexity of the curved surfaces is compared next for given inclination angles. Three selected diameter ratios (or the convexities), $D/D_j = 5.0$, 10, and ∞, positioned inside and outside the potential core are considered separately. To facilitate the comparison, the abscissa is converted to the lateral distance from the geometrical stagnation point i.e., s/D_j instead of the azimuth angle.

3.4.1 Inside the Potential Core. At $\theta = 0$ deg (the normal impinging position), the local heat transfer distribution on the large cylinder ($D/D_j = 10.0$) follows that on the flat plate, including the consistent lateral location of the local minimum at $s/D_j = 1.5$ and the second peak at $s/D_j = 2.0$ (Fig. 11(*a*)) [1,9–11,13,29]. As the jet is inclined to $\theta = 45$ deg, the difference in the local heat transfer on the downhill side becomes evident: a higher heat transfer on the flat plate and a lower heat transfer on a cylinder with a smaller D/D_j ratio as plotted in Fig. 11(*b*). However, its difference on the uphill side is negligible. The lateral location for the primary peak, the local minimum, and the second peak is coincident. Only the magnitude of the local heat transfer on the downhill side varies.

To examine qualitatively why the higher local heat transfer is obtained from a curved surface with a larger D/D_j (e.g., the flat plate) on the downhill side, an infinitesimally small fluid element following the streamlines in the vicinity of the cylinder surface is considered. No discontinuity of the streamlines is caused due to flow separation and a pressure gradient along the circumference of the cylinder is insubstantial as indicated by the static pressure distribution in Fig. 8(*b*). Force balance on this element along the axis normal to the cylinder surface i.e., the n-axis gives

$$F = \rho \frac{V^2}{D/2} \tag{8a}$$

where F is the centripetal force toward the center of the cylinder and V is the nominal velocity component parallel to the cylinder

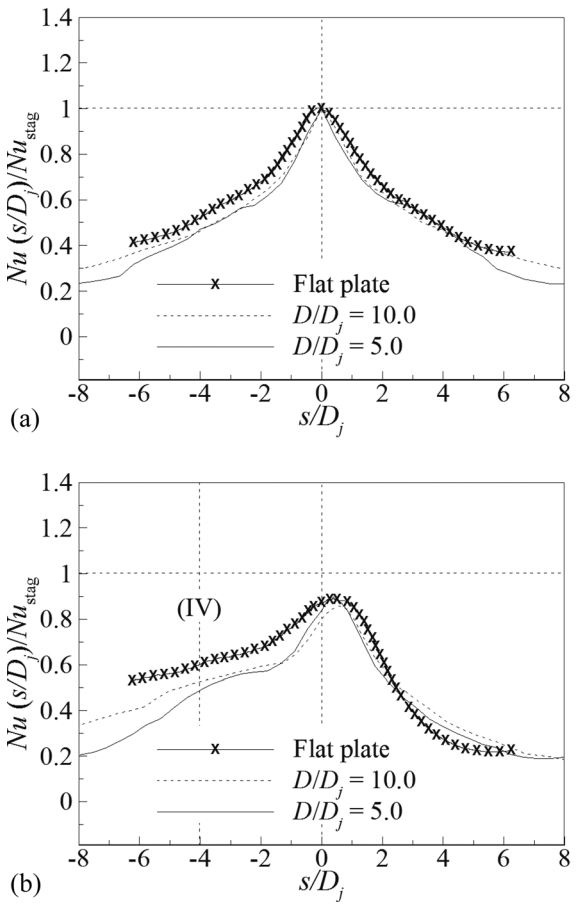

Fig. 13 Lateral heat transfer distribution on curved surfaces subject to an inclined impinging jet at $z/D_j = 8.0$ and $Re_j = 20{,}000$; (*a*) $\theta = 0$ deg; (*b*) $\theta = 45$ deg (location (IV) in Fig. 12)

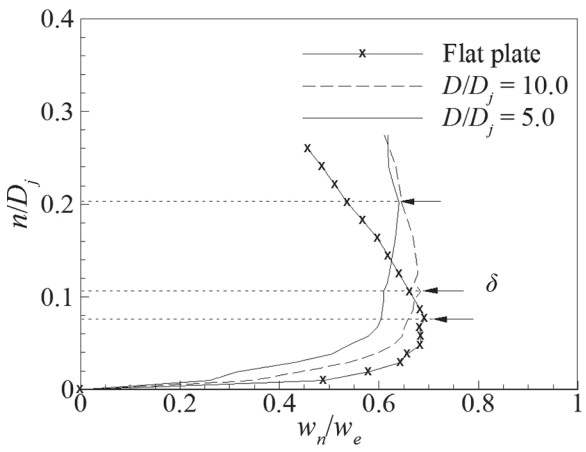

Fig. 14 Velocity profiles measured at $s/D_j = 4.0$ (denoted as (IV) in Fig. 12(*b*)) on two cylinders and a flat plate positioned at $z/D_j = 8.0$ (outside potential core)

surface. Velocity profiles in Fig. 12 measured downstream of the second peak i.e., $s/D_j = 4.0$ (indicated as (III) in Fig. 11(*b*)) demonstrate that the maximum flow velocity (taken as V in Eq. (8*a*)) is invariant i.e., $V =$ constant whereas the boundary layer is substantially thickened as the cylinder becomes smaller (e.g., $D/D_j = \infty \rightarrow D/D_j = 5.0$).

For a smaller cylinder, a greater centripetal force is required for balancing the centrifugal force to force the fluid element following the curved surface as

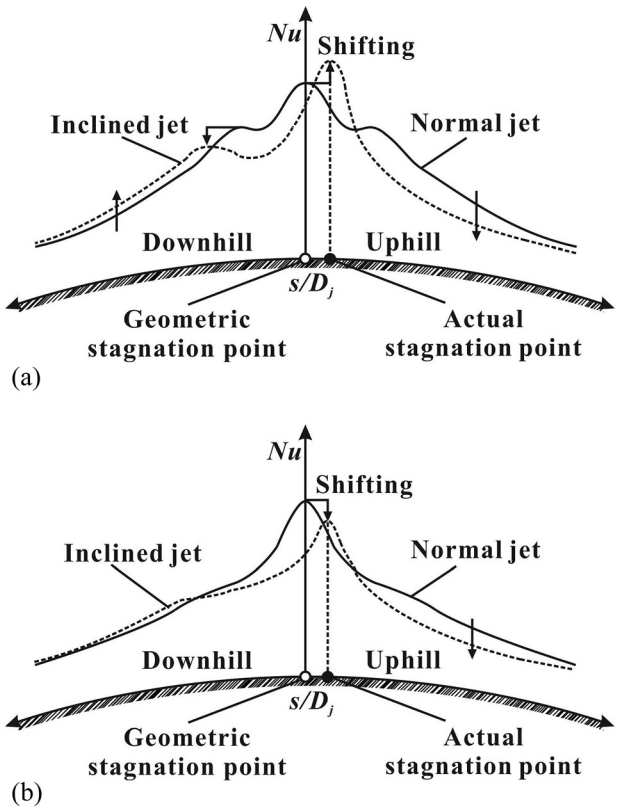

Fig. 15 Schematic summary illustrating how the inclination of a single circular jet affects azimuthal heat transfer distributions on a curved surface: (*a*) inside the potential core; (*b*) outside the potential core

$$F \sim \frac{1}{D/2} \tag{8b}$$

With $V =$ constant in Eq. (8*a*) irrespective of the D/D_j ratio, the centrifugal force is strengthened as the D/D_j ratio becomes smaller. The thickener boundary layer on a smaller cylinder (Fig. 12) indicates that the centripetal force F cannot balance the greater centrifugal force, which lifts the flow father away from the convexed surface. Hence, a further reduction of the local heat transfer is caused on the smaller cylinder surfaces as observed in Fig. 11(*b*); an upper bound is set by the flat plate. It should also be pointed out that the local Reynolds number based on the maximum flow velocity at $n/D_j = \delta$ remains unchanged: the local Reynolds number plays no part in influencing the local heat transfer.

3.4.2 Outside the Potential Core. Outside the potential core, the two cylinders almost follow the local distribution on the flat plate (Fig. 13(*a*)). The local heat transfer decreases monotonically from the stagnation point without forming a second peak. At $\theta = 45$ deg, the high heat transfer on the flat plate and the low heat transfer on the small cylinder as depicted in Fig. 13(*b*) whereas the negligible change of the local heat transfer is observed on the uphill side.

Similar to the observation on the cylinder positioned inside the potential core, the flow that undergoes the transition on the downhill side is influenced by the centrifugal force which pushes the flow away from the cylinder surface as inferred by the thickened boundary layer (Fig. 14 at the lateral location of $s/D_j = 4.0$ i.e., (IV) indicated in Fig. 13(*b*)). As a result, the local heat transfer is reduced on the small cylinder. It should also be pointed out that the local Reynolds number based on the maximum flow velocity at $n/D_j = \delta$ remains almost unchanged.

4 Conclusions

Details of local heat transfer characteristics on curved surfaces emitting constant heat flux subject to an inclined jet were considered at a fixed jet Reynolds number. Particular focus was placed on the effects of the inclination, the relative impinging distance to the potential core of jet flow, and the convexity of the target surfaces on local heat transfer characteristics. Similar and dissimilar characteristics on the curved surfaces to the flat plate were identified. New findings in this study are summarized with schematic illustrations in Fig. 15 as follows:

(1) There is a transitional response of the stagnation heat transfer (the primary peak) to the inclination, depending on the relative stream-wise location of a target surface to the potential core of jet flow.
(2) Inside the potential core, the primary peak that initially coincides with the geometric stagnation point shifts toward the uphill side with an increase in its magnitude as the inclination angle is increased regardless of the convexity of curved surfaces (Fig. 15(*a*)).
(3) Outside the potential core, the primary peak that shifts toward the uphill side is conversely decreased as the inclination angle is increased regardless of the convexity of curved surfaces (Fig. 15(*b*)).
(4) With the normal impinging jet, the second peak is formed only positioned inside the potential core. With the inclination, it disappears on the uphill side while that on the downhill side remains (Fig. 15(*a*)).
(5) Inside the potential core, the second peak on the downhill side is decreased with the inclination whereas that on the flat plate conversely increases (Fig. 15(*a*)). This is attributable to the thickening of the boundary layer whose extent is greater on small cylinders.

Acknowledgment

This study was supported by the Korea Ministry of Science and Technology via the South Korea-South Africa Research Center Program (Grant No.: 0420-20110129), by the NRF South Africa Incentive Fund for rated researchers, by the National Basic Research Program of China (Grant No.: 2011CB610305), the National 111 Project of China (Grant No.: B06024), China Postdoctoral Science Foundation funded project (2012M521766) and the Fundamental Research Funds for the Central Universities of China.

Nomenclature

C_p = Static pressure coefficient defined in Eq. (2)
D = circular cylinder diameter (m)
D_j = circular jet diameter (m)
F = centripetal force (N)
h = convective heat transfer coefficient (W/(m^{2}K))
k_f = thermal conductivity of air (W/(mK))
n = coordinate perpendicular to a target surface
Nu = Nusselt number based on a jet diameter defined in Eq. (3)
$p(\alpha)$ = pressure measured at an arbitrary azimuth angle (Pa)
p_e = static pressure measured at a jet exit (Pa)
q'' = net heat flux (W/m^2)
q''_{cond} = conductive heat loss (W/m^2)
q''_{input} = input heat flux (W/m^2)
q''_{rad} = radiative heat loss (W/m^2)
$\dot{m}$ = mass flow rate (kg/s)
Re_j = Reynolds number based on a jet diameter defined in Eq. (1)
s = lateral distance from the geometrical stagnation point (m)
T_a = ambient temperature (K)
T_j = jet temperature measured at jet exit (K)
T_s = local surface temperature measured on a circular cylinder or a flat plate (K)
w = axial velocity component of jet flow discharged from circular jet (m/s)
w_e = jet exit velocity at $r = 0$ and $z = 0$ (m/s)
w_m = mean jet velocity (m/s)
w_n = axial velocity along the n-coordinate
w_0 = centerline (axial) velocity at $r = 0$ (m/s)
w_r = jet velocity at a selected radial location (m/s)
z = axial coordinate coinciding with a jet axis
α = azimuth angle measured from a geometrical stagnation point (deg)
δ = boundary layer thickness (m)
ε = emissivity
θ = inclination angle (degree)
μ = viscosity of air (kg/(ms))
ρ = density of air (kg/m^3)
σ = Stefan–Boltzmann constant

References

[1] Gauntner, J. W., Livingood, J. N. B., and Hrycak, P., 1970, "Survey of Literature on Flow Characteristics of a Single Turbulent Jet Impinging on a Flat Plate," NASA TN D-5652 NTIS N70-1896
[2] De Wrachien, D., Lorenzini, G., and Medici, M., 2013, "Sprinkler Irrigation Systems: State-of-the-Art of Kinematic Analysis and Quantum Mechanics Applied to Water Jets," Irrigation Drainage, **62**(4), pp. 407–413.
[3] Lorenzini, G., and Saro, O., 2013, "Thermal Fluid Dynamic Modeling of a Water Droplet Evaporating in Air," Int. J. Heat Mass Transfer, **62**, pp. 323–335.
[4] Baughn, J., and Shimizu, S., 1989, "Heat Transfer Measurements From a Surface With Uniform Heat Flux and an Impinging Jet," ASME J. Heat Transfer, **111**(4), pp. 1096–1098.
[5] Baughn, J. W., Hechanova, A. E., and Yan, X., 1991, "An Experimental Study of Entrainment Effects on the Heat Transfer From a Flat Surface to a Heated Circular Impinging Jet," ASME J. Heat Transfer, **113**(4), pp. 1023–1025.
[6] Vipat, O., Feng, S. S., Kim, T., Pradeep, A. M., and Lu, T. J., 2009, "Asymmetric Entrainment Effect on the Local Surface Temperature of a Flat Plate Heated by an Obliquely Impinging Two-Dimensional Jet," Int. J. Heat Mass Transfer, **52**(21–22), pp. 5250–5257.
[7] Behnia, M., Parneix, S., Shabany, Y., and Durbin, P., 1999, "Numerical Study of Turbulent Heat Transfer in Confined and Unconfined Impinging Jets," Int. J. Heat Fluid Flow, **20**(1), pp. 1–9.
[8] Yang, H. Q., Kim, T., Lu, T. J., and Ichimiya, K., 2010, "Flow Structure, Wall Pressure and Heat Transfer Characteristics of Impinging Annular Jet With/Without Steady Swirling," Int. J. Heat Mass Transfer, **53**(19–20), pp. 4092–4100.
[9] Martin, H., 1977, "Heat and Mass Transfer Between Impinging Gas Jets and Solid Surfaces," Adv. Heat Transfer, **13**, pp. 1–60.
[10] Jambunathan, K., Lai, E., Moss, M. A., and Button, B. L., 1992, "A Review of Heat-Transfer Data for Single Circular Jet Impingement," Int. J. Heat Fluid Flow, **13**(2), pp. 106–115.
[11] Zuckerman, N., and Lior, N., 2006, "Jet Impingement Heat Transfer: Physics, Correlations, and Numerical Modeling," Adv. Heat Transfer, **39**, pp. 565–631.
[12] Livingood, J. N. B., and Hrycak, P., 1973, "Impingement Heat Transfer From Turbulent Air Jets to Flat Plates—A Literature Survey," NASA, TM X-2778.
[13] Gardon, R., and Akfirat, J. C., 1965, "The Role of Turbulence in Determining the Heat-Transfer Characteristics of Impinging Jets," Int. J. Heat Mass Transfer, **8**(10), pp. 1261–1272.
[14] Hofmann, H. M., Kind, M., and Martin, H., 2007, "Measurements on Steady State Heat Transfer and Flow Structure and New Correlations for Heat and Mass Transfer in Submerged Impinging Jets," Int. J. Heat Mass Transfer, **50**(19–20), pp. 3957–3965.
[15] Akansu, Y. E., Sarioglu, M., Kuvvet, K., and Yavuz, T., 2008, "Flow Field and Heat Transfer Characteristics in an Oblique Slot Jet Impinging on a Flat Plate," Int. Commun. Heat Mass Transfer, **35**(7), pp. 873–880.
[16] Goldstein, R., and Franchett, M., 1988, "Heat Transfer From a Flat Surface to an Oblique Impinging Jet," ASME J. Heat Transfer, **110**, pp. 84–90.
[17] Beitelmal, A. H., Saad, M. A., and Patel, C. D., 2000, "The Effect of Inclination on the Heat Transfer Between a Flat Surface and an Impinging Two-Dimensional Air Jet," Int. J. Heat Fluid Flow, **21**(2), pp. 156–163.
[18] Sparrow, E., and Lovell, B., 1980, "Heat Transfer Characteristics of an Obliquely Impinging Circular Jet," ASME J. Heat Transfer, **102**, pp. 202–209.
[19] Tong, A. Y., 2003, "On the Impingement Heat Transfer of an Oblique Free Surface Plane Jet," Int. J. Heat Mass Transfer, **46**(11), pp. 2077–2085.
[20] Yan, X., and Saniei, N., 1997, "Heat Transfer from an Obliquely Impinging Circular, Air Jet to a Flat Plate," Int. J. Heat Fluid Flow, **18**(6), pp. 591–599.
[21] Schueren, S., Hoefler, F., Von Wolfersdorf, J., and Naik, S., 2011, "Heat Transfer in an Oblique Jet Impingement Configuration With Varying Jet Geometries," ASME J. Turbomach., **135**(2), p. 021010.
[22] Gau, C., and Chung, C. M., 1991, "Surface Curvature Effect on Slot-Air-Jet Impingement Cooling Flow and Heat-Transfer Process," ASME J. Heat Transfer, **113**(4), pp. 858–864.

[23] Cornaro, C., Fleischer, A. S., Rounds, M., and Goldstein, R. J., 2001, "Jet Impingement Cooling of a Convex Semi-Cylindrical Surface," Int. J. Therm. Sci., **40**(10), pp. 890–898.
[24] Cornaro, C., Fleischer, A. S., and Goldstein, R. J., 1999, "Flow Visualization of a Round Jet Impinging on Cylindrical Surfaces," Exp. Therm. Fluid Sci., **20**(2), pp. 66–78.
[25] Lee, D. H., Chung, Y. S., and Kim, D. S., 1997, "Turbulent Flow and Heat Transfer Measurements on a Curved Surface With a Fully Developed Round Impinging Jet," Int. J. Heat Fluid Flow, **18**(1), pp. 160–169.
[26] Sparrow, E. M., Altemani, C. A. C., and Chaboki, A., 1984, "Jet-Impingement Heat-Transfer for a Circular Jet Impinging in Crossflow on a Cylinder," ASME J. Heat Transfer, **106**(3), pp. 570–577.
[27] Tawfek, A. A., 1999, "Heat Transfer Due to a Round Jet Impinging Normal to a Circular Cylinder," Heat Mass Transfer, **35**(4), pp. 327–333.
[28] Wang, X. L., Motala, D., Lu, T. J., Song, S. J., and Kim, T., 2014, "Heat Transfer of a Circular Impinging Jet on a Circular Cylinder in Crossflow," Int. J. Therm. Sci., **78**, pp. 1–8.
[29] Lim, K. B., Lee, C. H., Sung, N. W., and Lee, S. H., 2007, "An Experimental Study on the Characteristics of Heat Transfer on the Turbulent Round Impingement Jet According to the Inclined Angle of Convex Surface Using the Liquid Crystal Transient Method," Exp. Therm. Fluid Sci., **31**(7), pp. 711–719.
[30] Tawfek, A. A., 2002, "Heat Transfer Studies of the Oblique Impingement of Round Jets Upon a Curved Surface," Heat Mass Transfer, **38**(6), pp. 467–475.
[31] Coleman, H. W., and Steele, W. G., 2009, *Experimentation, Validation, and Uncertainty Analysis for Engineers*, John Wiley & Sons, Hoboken, NJ.
[32] Abramovich, G. N., and Schindel, L. H., 1963, *The Theory of Turbulent Jets*, MIT, Cambridge, MA.
[33] Reungoat, D., Riviere, N., and Faure, J. P., 2007, "3D PIV and PLIF Measurement in Turbulent Mixing—Round Jet Impingement," J. Visual-Jpn., **10**(1), pp. 99–110.
[34] Giralt, F., Chia, C. J., and Trass, O., 1977, "Characterization of Impingement Region in an Axisymmetric Turbulent Jet," Ind. Eng. Chem. Fund., **16**(1), pp. 21–28.
[35] Lee, D. H., Song, J., and Jo, M. C., 2004, "The Effects of Nozzle Diameter on Impinging Jet Heat Transfer and Fluid Flow," ASME J. Heat Transfer, **126**(4), pp. 554–557.
[36] Nizou, P., 1981, "Heat and Momentum Transfer in a Plane Turbulent Wall Jet," ASME J. Heat Transfer, **103**(1), pp. 138–140.